

Current invariant as fundamental relation between saturation currents and band gaps for semiconductor solar cells



Mikhail A. Mintairov*, Valery V. Evstropov, Sergey A. Mintairov, Mariia V. Nakhimovich, Roman A. Salii, Maxim Z. Shvarts, Nikolay A. Kalyuzhnyy

Ioffe Institute, 26 Polytechnicheskaya str., St.-Petersburg, 194021, Russia

ARTICLE INFO

Keywords:

Multi-junction solar cells
Current-voltage characteristics
Open circuit voltage
Voltage offset
Saturation current
Current invariants

ABSTRACT

The optimization of present multijunction junction solar cells and the development of new concepts is an important task for modern photovoltaics. For its development, special attention should be paid to the potential quality of photoactive *p-n* junctions, as well as to their properties when operating at various temperatures. The present research has shown that for two-diode model of the *p-n* junction it is convenient to use current invariants J_{z1} and J_{z2} for calculating the diffusion and recombination saturation dark currents J_{01} and J_{02} for *p-n* junctions based on semiconductor materials with any band-gap energy. It has been experimentally found that J_{z1} and J_{z2} are constants relating the semiconductor material band gap energy and temperature with J_{01} and J_{02} . It has also been shown that J_{z1} and J_{z2} determine the open circuit voltage and the value of voltage offset W_{OC} . Current invariant suggested to be useful tool for evaluating the quality of a *p-n* junction and for modeling the characteristics of solar cells because it allows making calculations taking into account both main mechanisms of current flow and the operating temperature of the device.

1. Introduction

The development of solar cells imposes new requirements on the cost and efficiency of the devices being created. The main approach for achieving super-high efficiency solar cells (SCs) is the use of multi-junction solar cells (MJ SC) [1]. The current trend in the design of semiconductor A^3B^5 SCs is that the number of *p-n* junctions is increased, while the band gap energy (E_g) of each *p-n* junction is optimized for the most efficient conversion of equal parts of the energy of the solar spectrum. Thus, besides the classical triple-junction SCs [2–5], 4-junction [6], 5-junction [7,8], and 6-junction [9] MJ SCs have been actively developed recently. In addition, other technologies of semiconductor MJ SCs have been developed, such as III-V/Si [10,11], II-VI/Si [12], CZTS/Si [13], and III-V/CIGSe [14]. Reducing the energy cost is one of the main goals of MJ SCs research which meets the problem that the predicted values of conversion efficiency have not yet been achieved [1]. This is partly due to the fact that basic calculations of optimal combinations of the E_g of subcells materials are based on a number of idealizations and overestimate the efficiency values. The main idealization is the dominance of interband recombination over recombination through deep levels in the *p-n* junction because most of

the models [2,15–19] are based on the calculations presented by Shockley-Queisser [20] and on the so-called detailed balance principle or on the methods directly arising from it [19,21–23]. However, the Shockley-Queisser method itself takes into account only radiative interband recombination. Another reason that the efficiency of modern MJ SCs does not reach its limiting (calculated) values is a number of technological problems. For example, the most industrially widespread GaInP/InGaAs/Ge triple-junction SCs is the result of compromises although the subcells' E_g differ significantly from the optimal calculated values. The above example concerned only triple-junction SCs, but one can expect similar variability for 4-, 5-, and 6-junction SCs as well as for SCs with larger number of subcells.

Thus, in the near future, the research of new combinations of subcells' materials will be relevant. It should be noted that, in fact, ongoing research are focused to searching only for combinations of E_g . Indeed, it is the main parameters for calculating the efficiency of SCs because it is E_g that determines the main fundamental losses during the absorption of light by a *p-n* junction: transparency of the semiconductor material for the photons with energies lower than E_g and thermalization losses of the part of the photon energy exceeding E_g . As a result, E_g directly sets the photogenerated current (J_g) of a subcell. From the other hand, E_g

* Corresponding author.

E-mail address: Mamint@mail.ioffe.ru (M.A. Mintairov).

determines the splitting of Fermi quasi-levels, i.e., determines the value of the open circuit voltage (V_{OC}) of SC. The existence of a simple relationship between V_{OC} and E_g was experimentally and theoretically studied as voltage offset ($W_{OC} = E_g/q - V_{OC}$) [24], where W_{OC} value for typical SCs under standard measurement conditions is close to a constant.

Recently we have shown that W_{OC} can be considered as a constant for typical SCs because there are fundamental dependencies of J_{01} – the diffusion (ideal Shockley, diode ideality coefficient $A = 1$) and J_{02} – the recombination (Shockley-Hall-Read, $A = 2$) p - n junction saturation currents on E_g Ref. [25]. Such experimental dependences for $In_xGa_{1-x}As$ SCs in the E_g range of 0.95–1.42 eV have been demonstrated and it has been shown that J_{01} and J_{02} , as well as W_{OC} , are determined by the constant value, which was named the current invariant J_z . The current invariant has an important advantage over the voltage offset because the latter depends on the SCs photogenerated current at which it is measured while J_z has no such dependency. In Ref. [26] we have also shown that J_z is independent on temperature for a GaAs SCs. In the present paper we present the research of the J_z for wide range of III-V semiconductors with E_g (0.74–1.9 eV) and for wide range of temperatures (100–424 K). All investigated semiconductors materials play an important role in the creation of subcells in MJ SCs and photoconverters of various types. Fundamental parameters J_{01} and J_{02} have been studied for SCs based on $Ga_{0.52}In_{0.48}P$ ($E_g \approx 1.90$ eV), GaAs ($E_g \approx 1.42$ eV), $In_{0.26}Ga_{0.74}As$ ($E_g \approx 1.06$ eV) and $In_{0.47}Ga_{0.53}As$ ($E_g \approx 0.74$ eV). An analysis of the dependences obtained has shown that both saturation currents are determined by their invariants J_{z1} and J_{z2} which are independent of temperature and E_g . The experimental temperature dependence of W_{OC} has also been obtained when the diffusion or the recombination mechanism of current flow dominates in the p - n junction. It has been shown that W_{OC} depends linearly on temperature and weakly depends on the type of the dominant current flow mechanism.

The main advantage of J_z is the possibility to carry out the realistic calculations of combinations of E_g for the subcells of MJ SC at different temperatures and illumination conditions. In the case of terrestrial 1-sun photovoltaics, SC always operates at the temperatures near 300 K with the dominance of the recombination mechanism of current flow. The space SCs have to be designed for operation at temperatures lower than 300K with dominance of recombination mechanism. For concentrating photovoltaics, the SC temperature can reach 340 K [27–29], and even more for laser power converters [30,31] and in these cases the diffusion mechanism dominates most often. The obtained values of the current invariant make it possible to investigate the optimal E_g combinations for all above mentioned conditions.

2. Experimental details and result discussion

2.1. Research objects and measuring equipment

The characteristics of four single-junction SCs were studied:

- 1 - $Ga_{0.52}In_{0.48}P$.
- 2 - GaAs.
- 3 - $In_{0.26}Ga_{0.74}As$.
- 4 - $In_{0.47}Ga_{0.53}As$.

All structures were grown using metal-organic vapor phase epitaxy and included a standard set of layers for SCs (back surface field, base, emitter, window, contact layer). Structures 1, 2, and 3 were grown on (100) GaAs substrates. Structures 1 and 2 were grown lattice-matched, structure 3 was grown on a metamorphic buffer [25], structure 4 was grown lattice-matched on (100) InP substrate.

As the third group element sources the following metalorganic compounds were used: trimethylgallium, trimethylaluminium and trimethylindium. Arsine and phosphine were used as the fifth group element sources, silane was used as an n -type impurity source, and

diethilzinc as p -type impurity source. Au:Ge/Ni/Au and Ag:Mn/Ni/Au metallisation were user for n - and p -type contact respectively. Face contact grid was made by photolithography and thickened by electrochemical deposition of gold up to thickness of about 2 μm . The cells dimensions were $3 \times 3 \text{ mm}^2$ with the contact grid spacing of 100 μm and shadowing of the order of 6 %. TiO_2/SiO_2 layers were used as an anti-reflection coating.

The following set of characteristics was measured for all samples:

- at $T = 300$ K dependence of V_{OC} on J_{SC} equal to photogenerated current (J_g).
- light IV curves at temperature range of 113–423 K (four IV curves for each temperature).
- electroluminescence intensity (EL) spectra at temperature range of 113–423 K.

Light IV characteristics were recorded using a Xenon flash tester. Spectral resolving device was used for EL measurements at direct current passing through p - n junctions. During measuring all characteristics, the samples were fixed on the heat sink by soldering. An optical cryostat with an input window was used for obtaining the temperature IV curves.

2.2. Current invariant: research technique and main experimental data

Diffusion (J_{01}) and recombination (J_{02}) dark saturation currents are proportional to the power function of temperature multiplied by the exponent [32]:

$$J_{01} = B_1 \cdot T^3 \exp\left(\frac{-E_g}{kT}\right) \quad (1)$$

$$J_{02} = B_2 \cdot T^{2.5} \exp\left(\frac{-E_g}{2kT}\right) \quad (2)$$

where k – the Boltzmann constant, T – the absolute temperature B_1 , B_2 – constants. Assuming the dominance of the exponential term in both equations over the power term and introducing the values of the current invariant J_{z1} for the diffusion current and J_{z2} for the recombination saturation current, one can obtain:

$$J_{0A} = J_{zA} \cdot \exp\left(\frac{-E_g}{AkT}\right), A = 1 \vee 2 \quad (3)$$

where A is ideality factor. Eq. (3) is based on the previous results [25, 26], where it was assumed that for typical SCs in a wide range of E_g and temperatures, the values of J_{01} and J_{02} are determined mainly by the exponential factor. In this case, both current invariants (J_{z1} and J_{z2}) are constants determining the basic relationship between the saturation currents and the value of E_g/T . Thus, according to our assumption, the current invariant for each current flow mechanism relates three quantities: saturation current, band gap energy, and temperature. To verify this assumption both dark saturation currents have been measured for a set of SCs at different temperatures.

As is known, the values of J_{01} and J_{02} can be easily found by approximating of a resistive-less dark IV characteristic using two-diode model [32]. In single-junction solar cells, the dependence of open-circuit voltage - short-circuit current (V_{OC} - J_g) can be used for this purpose:

$$J_g = J_{01} \cdot \exp\left(\frac{qV_{oc}}{kT}\right) + J_{02} \cdot \exp\left(\frac{qV_{oc}}{2kT}\right) \quad (4)$$

The experimental dependences for all samples, as well as the results of the approximation, are shown in Fig. 1. The contribution of each current flow mechanism is also shown in Fig. 1 (dashed lines). Three regions can be distinguished at V_{OC} - J_g characteristics:

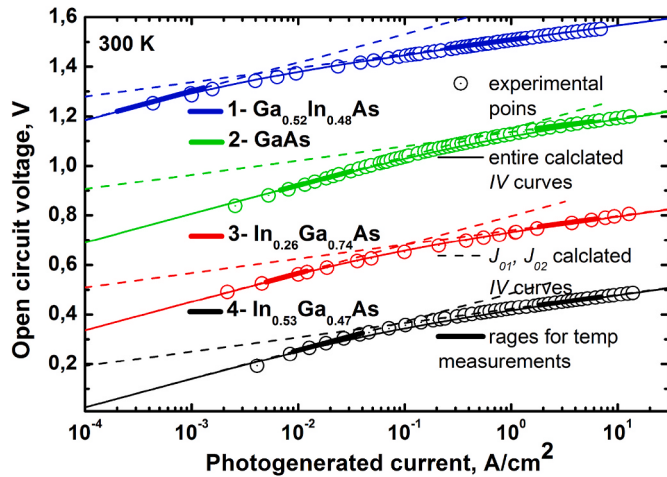


Fig. 1. Experimental (symbols) and calculated (lines) dependences V_{OC} - J_g (open circuit voltage - photogenerated current) for SCs based on $\text{Ga}_{0.52}\text{In}_{0.48}\text{P}$ (blue), GaAs (green), $\text{In}_{0.26}\text{Ga}_{0.74}\text{As}$ (red), and $\text{In}_{0.47}\text{Ga}_{0.53}\text{As}$ (black) obtained at room temperature. Solid thin lines - calculation according to the two-diode model, dotted lines - calculation of individual components of the two-diode model (Eq. (4)), thick lines show the current ranges in which the temperature measurements of the V_{OC} - J_g dependences (presented on Fig. 2) have been carried out.

Region 1 at low currents, the region in which the recombination mechanism of current flow dominates (the second term in Eq. (4) dominates over the first).

Region 2 where none of the current flow mechanisms can be neglected (none of the terms dominate).

Region 3 at high currents, the diffusion mechanism of current flow dominates (the first term in Eq. (3) dominates over the second).

In further measurements, we assumed that the current boundaries (Region 2) do not change significantly with temperature, which was finally confirmed experimentally. Therefore, for the task of measuring J_{01} and J_{02} , we measured several points of the V_{OC} - J_g dependence at currents in the Region 1 and Region 2 which are shown in Fig. 1 as thick lines.

After choosing the current measurement conditions, the samples have been placed in a cryostat, where they were first cooled down to a temperature of 113 K, and then heated to a temperature of 423 K and cooled again to room temperature. Thus, the entire temperature range of 113–423 K has been passed twice.

During the first pass, the IV characteristics have been measured at the currents corresponding to the range of dominance of the diffusion mechanism, while during the second pass, at the currents corresponding to the dominance of the recombination mechanism. Based on the measured IV characteristics for all samples, temperature V_{OC} - J_g dependences consisting of 4 points (2 points for each Range) have been plotted (Fig. 2).

As a result of the approximation by a two-diode model (lines in Fig. 2), the values of the saturation currents J_{01}, J_{02} were obtained for all temperatures. The EL spectra has been also measured during a change in temperature. The position of the maximum in the spectra was used to determine the E_g of a p - n junction. Fig. 3 shows the experimental temperature dependences of the E_g for all SCs under study. It is important to note that the resolution of the measuring device did not allow recording $\text{In}_{0.53}\text{Ga}_{0.47}\text{As}$ EL spectra for over the entire temperature range. However, the measured values are quite sufficient for accurate approximation of the obtained dependences using the Varshni formula [33]. The formula parameters for all SCs are shown in Table 1. The result of the

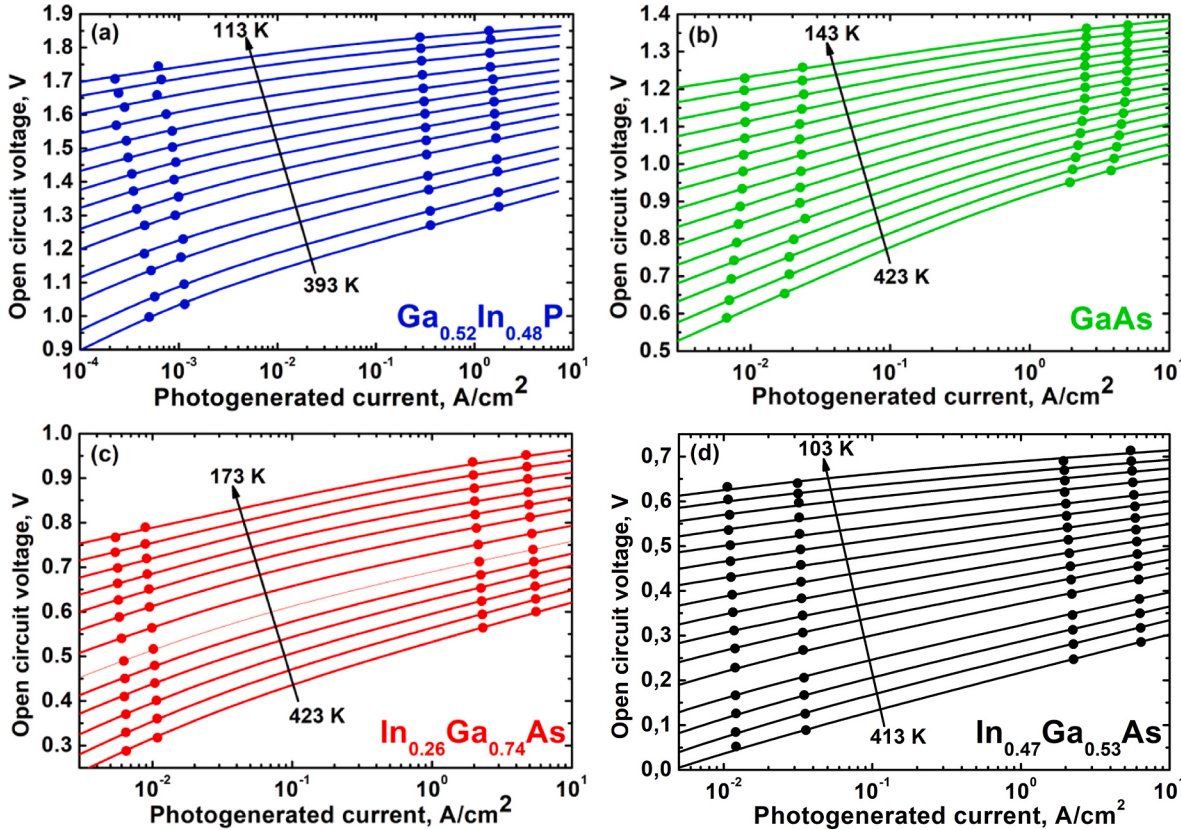


Fig. 2. Experimental (symbols) and calculated (lines) V_{OC} - J_g dependences obtained at different temperatures for SCs based on: $\text{Ga}_{0.52}\text{In}_{0.48}\text{P}$ (a), GaAs (b), $\text{In}_{0.26}\text{Ga}_{0.74}\text{As}$ (c), and $\text{In}_{0.47}\text{Ga}_{0.53}\text{As}$ (d). Solid lines - approximation by two-diode model.

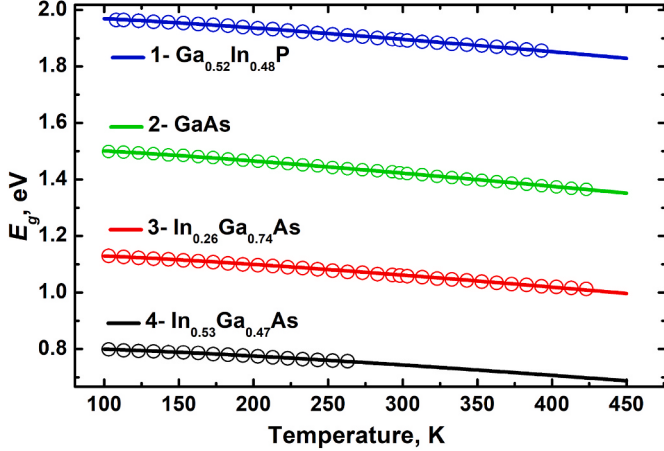


Fig. 3. Experimental (symbols) and calculated (lines) dependences of the E_g on temperature for SCs based on: $\text{Ga}_{0.52}\text{In}_{0.48}\text{P}$ (blue), GaAs (green), $\text{In}_{0.26}\text{Ga}_{0.74}\text{As}$ (red), and $\text{In}_{0.47}\text{Ga}_{0.53}\text{As}$ (black).

Table 1
Approximation parameters of the experimental dependences E_g on temperature (Fig. 3) according to the Varshni formula [32].

SC	E_{g0} , eV	Temperature corecipient, eV/K
$\text{Ga}_{0.52}\text{In}_{0.48}\text{P}$	1.985,	$5.405 \cdot 10^{-4}$
GaAs	1.519,	$5.405 \cdot 10^{-4}$
$\text{In}_{0.26}\text{Ga}_{0.74}\text{As}$	1.143,	$5.405 \cdot 10^{-4}$
$\text{In}_{0.47}\text{Ga}_{0.53}\text{As}$	0.810,	$5.005 \cdot 10^{-4}$

approximation is shown in Fig. 3 (lines). The resulting fitted data has been subsequently used to determine the E_g values for all samples, at temperatures corresponding to the J_{01} and J_{02} measurements.

2.3. Relation of temperature, saturation currents, band gap energy and voltage offset with the current invariant

Dependencies of the saturation currents on the value of E_g/T plotted in a semi-logarithmic scale (Fig. 4) summarize all the obtained experimental data. It is clearly seen that for both saturation currents all points lie around straight lines, which strictly corresponds to eq. (3). The calculation of J_{Z1} and J_{Z2} was carried out according to the reverse notation of equation (3) for all obtained experimental points:

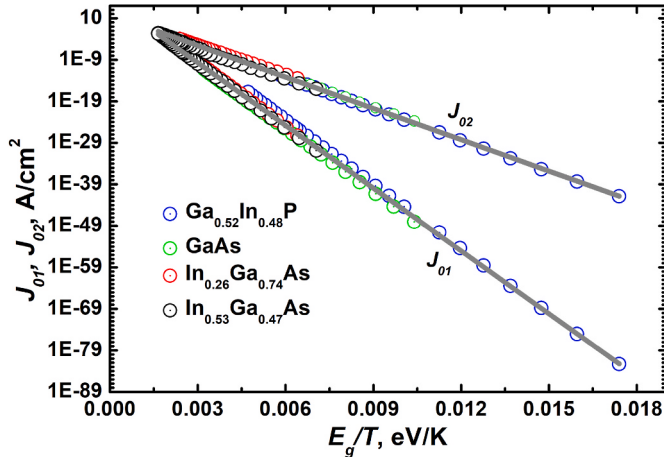


Fig. 4. Experimental (symbols) and calculated (lines) dependences of diffusion (J_{01}) and recombination (J_{02}) saturation currents on the E_g/T .

$$J_{zA} = \frac{J_{0A}}{\exp\left(\frac{-E_g}{AKT}\right)}, A = 1 \vee 2 \quad (5)$$

As a result, we have obtained the average value $J_{Z1} = 2.75 \cdot 10^5 \text{ A/cm}^2$ and $J_{Z2} = 98 \text{ A/cm}^2$. The calculated lines based on these values are shown in Fig. 4. The calculation has shown that the values of saturation currents obtained by eq. (3) deviate from the experimental ones by less than an order of magnitude. Thus, it can be argued that current invariants J_{Z1} and J_{Z2} relate E_g , temperature, and saturation dark currents. At the same time, the high accuracy of obtaining saturation currents makes it possible to calculate the IV characteristic of $p-n$ junctions for any E_g and temperature.

We also obtained and analyzed the temperature dependences of the voltage offset W_{OC} for all SCs under study. The voltage offset value is specified as $W_{OC} = E_g/q - V_{OC}$ [24]. The values of the voltage offset have been found based on the experimentally obtained values of J_{01} and J_{02} . Formally, there is no way to accurately determine the W_{OC} , because its value depends on the V_{OC} , which varies with the change in photogenerated current. The choice of photogenerated current is not strictly regulated, however, it is usual to measure it in the region of currents corresponding to the 1 sun incident radiation. In our case, we chose $J_g = 3 \cdot 10^{-3} \text{ A/cm}^2$ as the value of such photogenerated current. Further, using the calculated $V_{OC}-J_g$ dependences (Fig. 2), the value of V_{OC} was determined for each temperature, corresponding to $J_g = 3 \cdot 10^{-3} \text{ A/cm}^2$. The resulting W_{OC} temperature dependencies are shown in Fig. 5 (symbols).

W_{OC} has been calculated for two cases when the V_{OC} is determined only by diffusion or recombination current flow mechanisms. In case when one of the current flow mechanisms dominates in accordance with eq. (4) the V_{OC} is determined by the following expression:

$$V_{oc} = A \cdot \frac{kT}{q} \cdot \ln\left(\frac{J_g}{J_{0A}}\right), A = 1 \vee 2 \quad (6)$$

Substituting J_{0A} (3) into (6) one gets the following expression for V_{OC} :

$$V_{oc} = -A \cdot \frac{kT}{q} \cdot \ln\left(\frac{J_g}{J_{zA}}\right) + \frac{E_g}{q} = \frac{E_g}{q} - A \cdot \frac{kT}{q} \cdot \ln\left(\frac{J_{zA}}{J_g}\right), A = 1 \vee 2 \quad (7)$$

So, the W_{OC} is determined by the following expression:

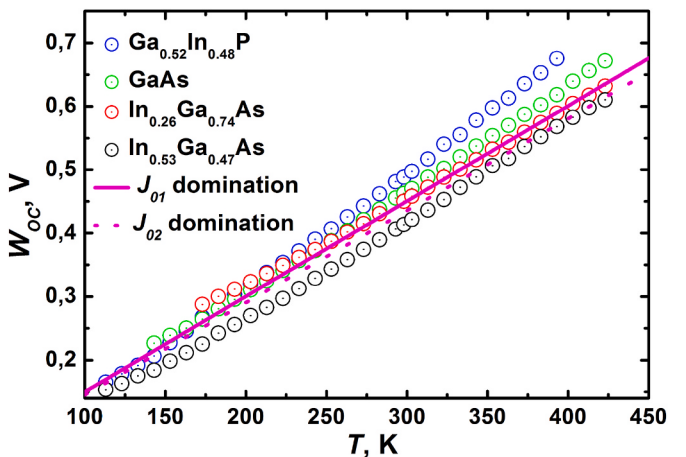


Fig. 5. Experimental (symbols) and calculated (lines) dependences of the voltage offset (W_{OC}) on temperature. Experimental dependences are obtained at current $J_g = 3 \cdot 10^{-3} \text{ A/cm}^2$ using $V_{OC}-J_g$ dependences (Fig. 2). The calculation was carried out according to eq. (8) for two cases: the solid line is the dominance of the diffusion mechanism of current flow ($A = 1$), the dotted line is the dominance of the recombination mechanism ($A = 2$).

$$W_{OC} = A \cdot \frac{kT}{q} \cdot \ln\left(\frac{J_{zA}}{J_g}\right), A = 1 \vee 2 \quad (8)$$

According to eq. (8), W_{OC} weakly (logarithmically) depends on the photogenerated current; therefore, at a given temperature, W_{OC} can be considered a constant if the current doesn't change on the orders of magnitude. In this case, its value is determined by the dominant current flow mechanism and, consequently, by the J_{Z1} or J_{Z2} . Fig. 5 shows the calculated temperature dependence of W_{OC} for both cases. It can be seen that the calculated values of W_{OC} for $A = 1$ and $A = 2$ differ but differ slightly. That is why one can say that at the room temperature the W_{OC} does not depend on the dominant current flow mechanism and is approximately equal to 0.45 V, which has been previously found by processing a large amount of experimental data [24]. In our research we have obtained the experimental value of 0.46 ± 0.05 V at a temperature of 300 ± 5 K.

Thus, the parameter W_{OC} can be determined by using the current invariant J_Z . In this case, W_{OC} linearly depends on temperature (eq. (8)), which has to be taken into account in numerical calculations, especially for space and concentrator SCs, where temperatures can differ significantly from room temperature. In addition, it should be noted that J_Z is determined more accurately because the deviation of experimental points for J_Z (Fig. 4) is much smaller than for W_{OC} (Fig. 5). Thus, in our opinion, the quality of the $p-n$ junction is better evaluating using the value of J_Z . On the other hand, the W_{OC} is a more practically convenient value, since it does not require the determination of saturation currents. But for modeling the characteristics of SCs, and in particular of MJ SCs, the use of J_Z is more promising, because it allows taking into account both main mechanisms of current flow and the operating temperature of the device.

2.4. Prediction of the dependences of diffusion and recombination saturation currents on the band gap at room temperature

As was noted above, the current invariants J_{Z1} and J_{Z2} make it possible to predict the saturation currents of $p-n$ junctions for typical SCs at any given temperature and for any E_g . This section compares the results of such a prediction with the published data.

The values of the invariants J_{Z1} and J_{Z2} found in the present research have been used in the calculations according to eq. (3) for the temperature $T = 298$ K. As a result, Fig. 6 shows the J_{01} and J_{02} values for the samples studied in the present research and the data for metamorphic InGaAs $p-n$ junctions [25], Ge SCs [34], Si SC [35] as well as for a 6-junction MJ SC [9]. The values of J_{02} are given for those $p-n$ junctions in

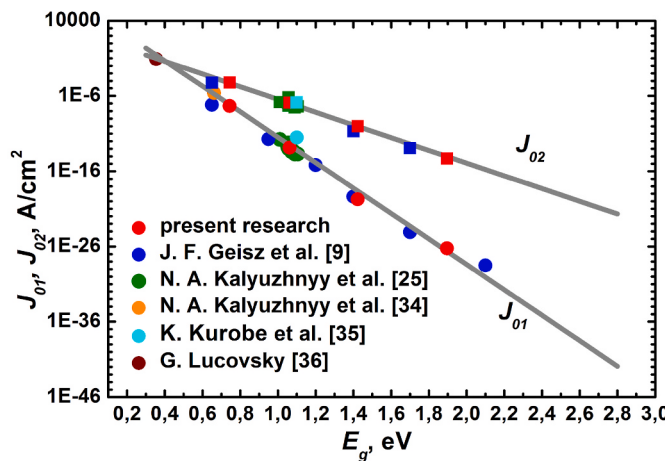


Fig. 6. Symbols: experimental values of saturation currents: J_{01} – circles, J_{02} , squares. The lines show the calculated dependences for both saturation currents obtained using eq. (3) and experimentally found values of J_{Z1} and J_{Z2} .

which the saturation current for the diode Shockley-Hall-Read ideality factor was strictly equal to 2. Finally, the experimental points of J_{01} for the narrow bandgap InAs $p-n$ junction is also presented [36]. It can be seen that the prediction of the J_{01} and J_{02} values is quite good in the entire presented range. On average, the experimental values deviate by less than an order of magnitude from calculated results. The maximum deviation for J_{01} did not exceed two orders of magnitude, and for J_{02} one. The observed deviations are due to the fact that in different semiconductors the material parameters that affect the value of the current invariant (effective mass, diffusion length, lifetime, mobility, etc.) may differ significantly. Evaluation using (7) (for room temperature) showed that the maximum deviation of the calculated values of the saturation currents corresponds to a change in the open-circuit voltage of 0.115 V. On average, using current invariants, the voltage of the subcells is determined with an accuracy of 0.057 V.

3. Conclusions

In the presented research, for SCs based on $\text{Ga}_{0.52}\text{In}_{0.48}\text{P}$, GaAs, $\text{In}_{0.26}\text{Ga}_{0.74}\text{As}$, and $\text{In}_{0.47}\text{Ga}_{0.53}\text{As}$ the temperature dependences of diffusion (J_{01}) and recombination (J_{02}) saturation currents on the E_g are experimentally obtained. The measurements were performed at the temperatures range of 113–423 K. An analysis of the experimental data has shown that, over the entire temperature range, the current invariants J_{Z1} and J_{Z2} , relating J_{01} and J_{02} to the value of E_g/T , can be considered as constants: $J_{Z1} = 2.75 \cdot 10^5 \text{ A}/\text{cm}^2$ and $J_{Z2} = 98 \text{ A}/\text{cm}^2$. The experimentally determined values of the saturation currents differed from the calculated ones by less than an order of magnitude, which proves the high accuracy of predicting these values. Thus, using the found values of J_{Z1} and J_{Z2} , it is possible to predict J_{01} and J_{02} and determine the IV characteristic of the SC for given E_g and temperature. This is especially important when finding the optimal materials for the next generation of high-efficient MJ SCs. Also, J_{Z1} and J_{Z2} are important metrics that characterize the basic quality of a $p-n$ junction and allow comparing $p-n$ junctions made of different materials. It has to be noted that the inclusion of the current invariant in the existing models for calculating the current-voltage characteristics of MJ SCs results in no additional difficulties, but significantly improves the resulting calculated characteristics closer to the experimental ones, which is a practically useful result.

The temperature dependence of the voltage offset W_{OC} has been also experimentally studied. It is shown that W_{OC} is proportional to the temperature and can be determined using the J_{Z1} and J_{Z2} . W_{OC} has been calculated for two cases: at the dominance of the diffusion mechanism of current flow (only J_{Z1} has been taken into account) and at the dominance of the recombination mechanism (only J_{Z2} has been taken into account). It has been shown that the dominant current flow mechanism has small effect on the value of W_{OC} . The calculated and experimentally determined value of W_{OC} at room temperature has been found to be 0.46 V.

For room temperature, a comparative analysis of the calculated saturation currents with experimental data available in open sources was carried out. It is shown that the calculation, using the current invariant, can predict the saturation currents of solar cells in a wide range of band gap energy 0.35–2.1 eV.

CRediT authorship contribution statement

Mikhail A. Mintairov: Writing – original draft, Project administration, Formal analysis, Data curation, Conceptualization. Valery V. Evstropov: Writing – review & editing, Writing – original draft, Formal analysis, Conceptualization. Sergey A. Mintairov: Writing – review & editing, Visualization. Mariia V. Nakhimovich: Methodology, Data curation. Roman A. Salii: Writing – review & editing. Maxim Z. Shvarts: Writing – review & editing, Validation, Resources, Methodology, Investigation. Nikolay A. Kalyuzhnyy: Writing – review & editing,

Supervision, Data curation.

Declaration of competing interest

The authors declare that they have no known competing financial interests or personal relationships that could have appeared to influence the work reported in this paper.

Data availability

Data will be made available on request.

Acknowledgments

The research was supported by the Russian Science Foundation (Grant No-22-19-00158, <https://rscf.ru/en/project/22-19-00158/>).

References

- [1] M. Yamaguchi, F. Dimroth, J.F. Geisz, N.J. Ekins-Daukes, Multi-junction solar cells paving the way for super high-efficiency, *J. Appl. Phys.* 129 (24) (Jun. 2021), 240901, <https://doi.org/10.1063/5.0048653>.
- [2] R.R. King, et al., Band-gap-engineered Architectures for High-Efficiency Multijunction Concentrator Solar Cells, WIP-Munich, 2009, <https://doi.org/10.4229/24theupvsec2009-1ao.5.2>.
- [3] W. Guter, et al., Current-matched triple-junction solar cell reaching 41.1% conversion efficiency under concentrated sunlight, *Appl. Phys. Lett.* 94 (22) (Jun. 2009), 223504, <https://doi.org/10.1063/1.3148341>.
- [4] W. Guter, et al., III-V Multijunction Solar Cells Lattice-Matched Products and Development of Upright Metamorphic 3J Cells, 2011, pp. 5–8, <https://doi.org/10.1063/1.3658282>.
- [5] K. Sasaki, T. Agui, K. Nakaido, N. Takahashi, R. Onitsuka, T. Takamoto, Development of InGaP/GaAs/InGaAs Inverted Triple Junction Concentrator Solar Cells, 2013, pp. 22–25, <https://doi.org/10.1063/1.4822190>.
- [6] R.M. France, et al., Design flexibility of ultrahigh efficiency four-junction inverted metamorphic solar cells, *IEEE J. Photovoltaics* 6 (2) (Mar. 2016) 578–583, <https://doi.org/10.1109/JPHOTOV.2015.2505182>.
- [7] S.P. Philipps, F. Dimroth, A.W. Bett, High-efficiency III-v multijunction solar cells, in: *Mcevoy's Handbook of Photovoltaics*, Elsevier, 2018, pp. 439–472.
- [8] R.H. van Leest, D. Fuhrmann, A. Frey, M. Meusel, G. Siefer, S.K. Reichmuth, Recent progress of multi-junction solar cell development for CPV applications at AZUR SPACE, in: 15th International Conference on Concentrator Photovoltaic Systems (CPV-15), vol. 2149, 2019, 020007, <https://doi.org/10.1063/1.5124177>.
- [9] J.F. Geisz, et al., Six-junction III-v solar cells with 47.1% conversion efficiency under 143 suns concentration, *Nat. Energy* 5 (4) (Apr. 2020) 326–335, <https://doi.org/10.1038/s41560-020-0598-5>.
- [10] S. Essig, et al., Raising the one-sun conversion efficiency of III-v/si solar cells to 32.8% for two junctions and 35.9% for three junctions, *Nat. Energy* 2 (9) (Aug. 2017), 17144, <https://doi.org/10.1038/nenergy.2017.144>.
- [11] D. Lackner, et al., Two-terminal direct wafer-bonded GaInP/AlGaAs/si triple-junction solar cell with AM1.5g efficiency of 34.1, *Sol. RRL* 4 (9) (Sep. 2020), 2000210, <https://doi.org/10.1002/solr.202000210>.
- [12] M. Carmody, et al., Single-crystal II-VI on si single-junction and tandem solar cells, *Appl. Phys. Lett.* 96 (15) (Apr. 2010), 153502, <https://doi.org/10.1063/1.3386529>.
- [13] K. Makita, et al., III-v/si multijunction solar cells with 30% efficiency using smart stack technology with pd nanoparticle array, *Prog. Photovoltaics Res. Appl.* 28 (1) (Jan. 2020) 16–24, <https://doi.org/10.1002/pip.3200>.
- [14] M. Valentini, et al., Fabrication of monolithic CZTS/si tandem cells by development of the intermediate connection, *Sol. Energy* 190 (Sep. 2019) 414–419, <https://doi.org/10.1016/j.solener.2019.08.029>.
- [15] D.N. Micha, R.T. Silvares Junior, The influence of solar spectrum and concentration factor on the material choice and the efficiency of multijunction solar cells, *Sci. Rep.* 9 (1) (Dec. 2019), 20055, <https://doi.org/10.1038/s41598-019-56457-0>.
- [16] J. Zeitouny, E.A. Katz, A. Dollet, A. Vossier, Band gap engineering of multi-junction solar cells: effects of series resistances and solar concentration, *Sci. Rep.* 7 (1) (May 2017) 1766, <https://doi.org/10.1038/s41598-017-01854-6>.
- [17] R.R. King, et al., 40% efficient metamorphic GaInP/GaInAs/ge multijunction solar cells, *Appl. Phys. Lett.* 90 (18) (Apr. 2007), 183516, <https://doi.org/10.1063/1.2734507>.
- [18] I. Tobías, A. Luque, Ideal efficiency of monolithic, series-connected multijunction solar cells, *Prog. Photovoltaics Res. Appl.* 10 (5) (Aug. 2002) 323–329, <https://doi.org/10.1002/pip.427>.
- [19] C.H. Henry, Limiting efficiencies of ideal single and multiple energy gap terrestrial solar cells, *J. Appl. Phys.* 51 (8) (1980) 4494, <https://doi.org/10.1063/1.328272>.
- [20] W. Shockley, H.J. Queisser, Detailed balance limit of efficiency of p-n junction solar cells, *J. Appl. Phys.* 32 (3) (1961) 510, <https://doi.org/10.1063/1.1736034>.
- [21] G. Letay, A. Bett, EtaOpt – a Program for Calculating Limiting Efficiency and Optimum Bandgap Structure for Multi-Bandgap Solar Cells and TPV Cells, Oct. 2001 [Online]. (Accessed 14 October 2020).
- [22] P.T. Landsberg, P. Baruch, The thermodynamics of the conversion of radiation energy for photovoltaics, *J. Phys. Math. Gen.* 22 (11) (Jun. 1989) 1911–1926, <https://doi.org/10.1088/0305-4470/22/11/028>.
- [23] A.D. Vos, Detailed balance limit of the efficiency of tandem solar cells, *J. Phys. Appl. Phys.* 13 (5) (May 1980) 839–846, <https://doi.org/10.1088/0022-3727/13/5/018>.
- [24] R.R. King, et al., Band gap-voltage offset and energy production in next-generation multijunction solar cells, *Prog. Photovoltaics Res. Appl.* 19 (7) (Nov. 2011) 797–812, <https://doi.org/10.1002/pip.1044>.
- [25] N.A. Kalyuzhnny, et al., Optimization of photoelectric parameters of InGaAs metamorphic laser (nm) power converters with over 50% efficiency, *Sol. Energy Mater. Sol. Cell.* 217 (Nov. 2020), 110710, <https://doi.org/10.1016/j.solmat.2020.110710>.
- [26] M.A. Mintairov, V.V. Evstropov, S.A. Mintairov, M.V. Nakhimovich, M.Z. Shvarts, N.A. Kalyuzhnny, The GaAs laser photoconverter (nm) current flow mechanisms at the temperature range of 100–420 k, *J. Phys. Conf.* 1697 (1) (Dec. 2020), 012170, <https://doi.org/10.1088/1742-6596/1697/1/012170>.
- [27] V.D. Rumyantsev, et al., Cell Chip Temperature Measurements in Different Operation Regimes of HCPV Modules, 2013, pp. 138–141, <https://doi.org/10.1063/1.4822217>.
- [28] M.A. Steiner, J.F. Geisz, D.J. Friedman, W.J. Olavarria, A. Duda, T.E. Moriarty, Temperature-dependent measurements of an inverted metamorphic multijunction (IMM) solar cell, in: 2011 37th IEEE Photovoltaic Specialists Conference, Jun. 2011, <https://doi.org/10.1109/PVSC.2011.6186461>, 002527–002532.
- [29] J. Jaus, R. Hue, M. Wiesenfarth, G. Peharz, A.W. Bett, Thermal Management in a Passively Cooled Concentrator Photovoltaic Module, WIP-Munich, 2008, <https://doi.org/10.4229/23deupvsec2008-1dv.3.23>.
- [30] O. Hohn, A.W. Walker, A.W. Bett, H. Helmers, Optimal laser wavelength for efficient laser power converter operation over temperature, *Appl. Phys. Lett.* 108 (2016), 241104, <https://doi.org/10.1063/1.4954014>.
- [31] M.Z. Shvarts, V.M. Emelyanov, D.A. Malevskiy, M.A. Mintairov, S.A. Mintairov, M. V. Nakhimovich, P.V. Pokrovskiy, R.A. Salii, N.A. Kalyuzhnny, “Temperature tweaking of the output photovoltaic parameters of laser power converters”, *IEEE Electron. Device Lett.* 41 (2020) 1324–1327, <https://doi.org/10.1109/LED.2020.3012023>.
- [32] G. Siefer, A.W. Bett, Analysis of temperature coefficients for III-v multi-junction concentrator cells, *Prog. Photovoltaics Res. Appl.* 22 (5) (May 2014) 515–524, <https://doi.org/10.1002/pip.2285>.
- [33] Y.P. Varshni, Temperature dependence of the energy gap in semiconductors, *Physica* 34 (1) (Jan. 1967) 149–154, [https://doi.org/10.1016/0031-8914\(67\)90062-6](https://doi.org/10.1016/0031-8914(67)90062-6).
- [34] N.A. Kalyuzhnny, et al., Germanium subcells for multijunction GaInP/GaInAs/ge solar cells, *Semiconductors* 44 (11) (Nov. 2010) 1520–1528, <https://doi.org/10.1134/S106378261011028X>.
- [35] K. Kurobe, H. Matsunami, New two-diode model for detailed analysis of multicrystalline silicon solar cells, *Jpn. J. Appl. Phys.* 44 (No. 12) (2005) 8314–8321, <https://doi.org/10.1143/JJAP.44.8314>.
- [36] G. Lucovsky, Electrical characteristics of diffused InAs p-n junctions, *Br. J. Appl. Phys.* 12 (6) (Jun. 1961) 311–312, <https://doi.org/10.1088/0508-3443/12/6/111>.